GEOMORPHIC POINT CLOUD DATA PROCESSING BASED ON AMPLITUDE SEPARATION AND FUSION ALGORITHM

Chen TANG[1], Chen WANG[1], Chuan WAN[2]*, Maoyun ZHANG[1], Fenglong CHEN[1]

With the rapid development of laser technology and computer technology, terrain data is usually obtained by airborne LiDAR detection. In terrain data processing, bilateral filtering method is widely used, but the filtering speed and the efficiency of the method is low. Especially in the terrain with complex environment, the local noise of the data is very large, and it is difficult for the laser radar to detect effectively. In order to solve such problems, a new point cloud image segmentation algorithm is adopted in this paper. Based on different amplitude separation and fusion algorithms, the surface and non-surface are fused, the amplitude filtering of the ground point cloud is realized by means filtering, and the light smoothness and smoothness of the point cloud are realized by combining bilateral filters. Then the mean square error MSE value is used as the benchmark for testing. This method can effectively solve the problem of slow speed and low precision of bilateral filtering and provides a theoretical basis for solving the situation of large noise in terrain point cloud data.

Keywords: geomorphic point cloud; bilateral filtering algorithm; amplitude separation fusion algorithm

1. Introduction

In the process of terrain acquisition, LiDAR can effectively reflect the surface geometric features of the target object and accurately measure its relative stereoscopic information [1]. In addition, it will also carry the information of the surface reflection characteristics of the target object together, so as to obtain a more comprehensive spatial information of the target object. After data processing of these information, 3D surface modeling of the ground target can be realized [2] and it can be identified. Three-dimensional Lidar is an indispensable part of topography, and LiDAR can display the topography features of ground objects in the form of point clouds, but there is a large noise in the local ground objects acquired by LiDAR, which is the main problem at present.

[1] School of Mechanical and Electrical Engineering, Changchun University of Science and Technology, Changchun 130117, China
[2] School of Information Science and Technology, Northeast Normal University, Changchun 130117, China
* Correspondence author: Chuan Wan, e-mail: wanc100@nenu.edu.cn

At present, many researchers at home and abroad have given various methods for noise and smoothing in point cloud modeling. Zheng L., Yaowu Z., and Si Jing Z. [3] proposed an end-to-end network of PCDNF for point cloud denoising based on joint normal filtering and introduced an auxiliary normal filtering task to enhance the network's ability to retain geometric features more accurately while removing noise. Duan X, Feng L, Zhao X [4], using geometric measures on statistical manifolds, and based on local statistical characteristics between noise and effective data, by calculating the expectation and covariance matrix of data points, point clouds containing high-density noise are projected onto manifolds of Gaussian distribution family to form parametric point clouds for denoising. Sun W, Wang J, and Jin F [5] proposed a de-noising network for unknown scenes based on point cloud manifold features, using manifold features to ensure accurate estimation of noise offset and manifold de-noising to solve noise offset at different disturbance points. Vollmer applied Laplacian algorithm to point cloud denoising and moved data points to the center of gravity of local point cloud data through multiple iterations. However, Laplacian algorithm was suitable for models with relatively uniform point cloud distribution. For models with uneven distribution, multiple iterations would distort the point cloud model [6].

The filtering effect of the above algorithms is not ideal in the case of large geomorphic amplitude. Therefore, in order to reduce the impact of large amplitude on laser 3D geomorphic point cloud data, a 3D laser point cloud processing method based on different amplitude separation and fusion algorithm is proposed in this paper. The feasibility of the method is verified by experiments, and the effectiveness of the denoising algorithm is verified by comparison with the bilateral filtering algorithm, The specific process is shown in Fig. 1.

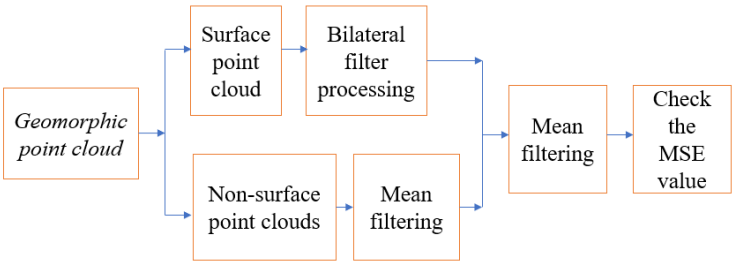

Fig. 1. Composite filtering process

2. Amplitude separation fusion algorithm

2.1 Bilateral filtering algorithm

The main idea of bilateral filtering is to make comprehensive use of the spatial and numerical information of the points to be filtered [7], so as to achieve effective protection of the boundary in point cloud smoothing. The conventional weighted average filtering algorithm can be represented by equation (1).

In formula (1), $I^*(p)$ and $I(p)$ represents the gray values of the front and rear pixels, $N(p)$ which is used to represent the neighborhood set of p, $W(q)$ represents the weighted weight of the neighborhood pixel q [8]. The two-sided filter weighting consists of the weighting of frequency domain and the weighting of number range preservation function represented by the weighting of Gaussian filter.

$$I^*(P) = \frac{\sum_{q \in N(p)} W(q) I(q)}{\sum_{q \in N(p)} W(q)} \tag{1}$$

Bilateral filtering calculation formula 2:

$$I^*(P) = \frac{\sum_{q \in N(P)} W_{\sigma_c}(|q-p|) W_{\sigma_x}(|I(q)-I(p)|) I(q)}{\sum_{q \in N(P)} W_{\sigma_c}(|q-p|) W_{\sigma_x}(|I(q)-I(p)|)} \tag{2}$$

In equation (2), p is the current point, W_{σ_c} and W_{σ_x} the weight function of.Gaussian filter is calculated by (3) and (4).

$$W_{\sigma_c} = e^{-\frac{y^2}{2\sigma_c}} \tag{3}$$

$$W_{\sigma_x} = e^{-\frac{x^2}{2\sigma_x}} \tag{4}$$

In formula (3) and (4), σ_c is the standard deviation of the spatial filtering weight function, and σ_x represents the standard deviation of the pixel correlation weight function.

2.2 Amplitude separation fusion filtering algorithm

Aiming at the characteristics of large terrain changes [9], this paper proposes a 3D point cloud data processing method based on different amplitude separation and fusion, The specific process is shown in Fig. 2, and realizes the following steps:

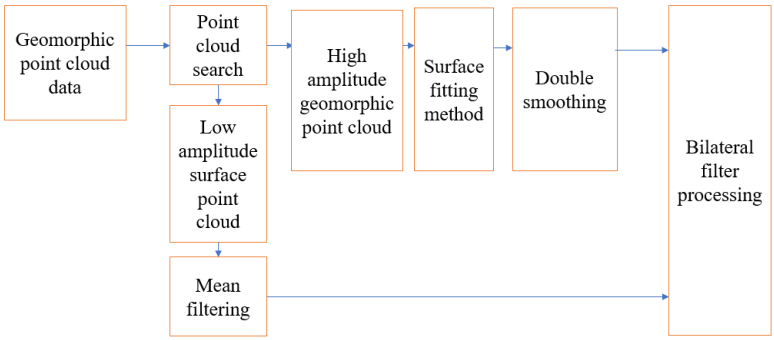

Fig. 2 Flow chart of amplitude separation

1) Arrange all the data in the point cloud according to the order of high and low, select the point with the smallest difference between high and low, and conduct large-area point cloud search [10]. When the difference between high and low changes, or the number of point clouds in a specific area decreases, the search will be terminated, and the level at the end of the search will be regarded as the level of division. On this basis, the extracted point cloud data is used as the surface [11], and the remaining point cloud data is used as the surface object. Two point cloud data are obtained by processing two point cloud data.

2) The surface fitting algorithm given in point cloud library PCL [12] is used to estimate the normal vector and curvature of each vertex in the pointcloud model of the cut object surface. In this paper, the estimation problem of point cloud normal vector is transformed into the fitting problem of least square method, and then the estimation problem ofpoint cloud normal vector [13] is transformed into the estimation problem of point cloud normal vector. By using the characteristics of kd-tree, a data structure that partitions K-dimensional data space, the neighboringpoints of a given target sample point, namely K neighborhood, can be quickly and accurately quepoints of a ried, and the required neighboring elements of target points can be provided for covariance matrix [14] *C*. Each target point has

$$C = \frac{1}{k}\sum_{p_i \in N(p_i)} \left(p_i - \vec{p}\right) \bullet (p_i - \vec{p})^T \tag{5}$$

$$C \bullet \overrightarrow{\upsilon_j} = \lambda_j \bullet \overrightarrow{\upsilon_j} j \in \{0,1,2\} \tag{6}$$

the following corresponding covariance matrix, as shown in formula (5) (6).

k is the number of elements [15] in the adjacent point p_i of the target point $N(p_i)$, $\vec{p}$ represents the three-dimensional centroid of the nearest neighbor element $N(p_i)$, which can be obtained from formula (7), λ_j is the j eigenvalue of the covariance matrix C, and υ_j is the j eigenvector.

υ_0 is the sampling point corresponding [16] to the smallest eigenroot λ_0 , and

$$\vec{p} = \frac{1}{k}\sum_{p_i \in N(p_i)} p_i \tag{7}$$

$p_i \in S$ approximates the normal vector. Through the normal vector estimation of the ground target, the normal vector estimation graph of the point cloud model is obtained.

Then the two-sided filter is used to smooth the point cloud data [17]. The bilateral filtering algorithm formula can be expressed by formula (8).

In equation (8), $\overrightarrow{n_i}$ is the normal vector of the filter point P_i , and the normal

$$P_i = P_i + \lambda \overrightarrow{n_i} \tag{8}$$

vector estimation of the point [18] has been obtained. λ is the filter factor and the adjustment factor of the filter point position. Similarly, the calculation process of the adjustment factor λ of the filter point position is derived as (9) [19].

$$\lambda = \frac{\sum_{P_j \in N_k(P_i)} W_C\left(P_j - P_i\right) W_s\left(\left\|\left(P_j - P_i\right), \overrightarrow{n_i}\text{-}1\right\|\right)\left(P_j - P_i\right), \overrightarrow{n_i}}{\sum_{P_j \in N_k(P_i)} W_C\left(P_j - P_i\right) W_s\left(\left\|\left(P_j - P_i\right), \overrightarrow{n_i}\text{-}1\right\|\right)} \tag{9}$$

W_C contained in formula (9) represents the calculated weight value of the operator in space and, W_S is the calculated [20] weight function value in the frequency domain, and $P_j - P_i, \overrightarrow{n_i}$ is the inner product of $\vec{n}_i$ and $P_j - P_i$.

In formula (10) and (11), $x = P_j - P_i$ [21] in the weight function calculation

$$W_C(x) = e^{-\frac{x^2}{2\sigma_c}} \tag{10}$$

$$W_S(y) = e^{-\frac{y^2}{2\sigma_s}} \tag{11}$$

formula represents the spatial distance between the fairing vertex Pi and the neighboring point, and $y = P_j - P_i, \overrightarrow{n_i}$ represents the projection on the normal vector $\overrightarrow{n_i}$ of the filtering point by the vector composed of the filtering point P_i and the neighboring point P_j.

3）The mean value of the separated ground is continued to be filtered, and the height value is distributed according to the position, and the mean value is filtered according to the average convolution of adjacent points. Then, the height value is combined with the ground target, and the ground is filtered bilaterally. At the same time, the separated ground is filtered bilaterally.

3. Experimental verification and simulation analysis

3.1 Geomorphic point cloud data acquisition

In this paper, a pulsed single-reflector laser 3D scanning measurement system is built, which is mainly composed of a laser transceiver system, a laser scanning system and a data post-processing system, etc. The specific structure is shown in Fig. 3.

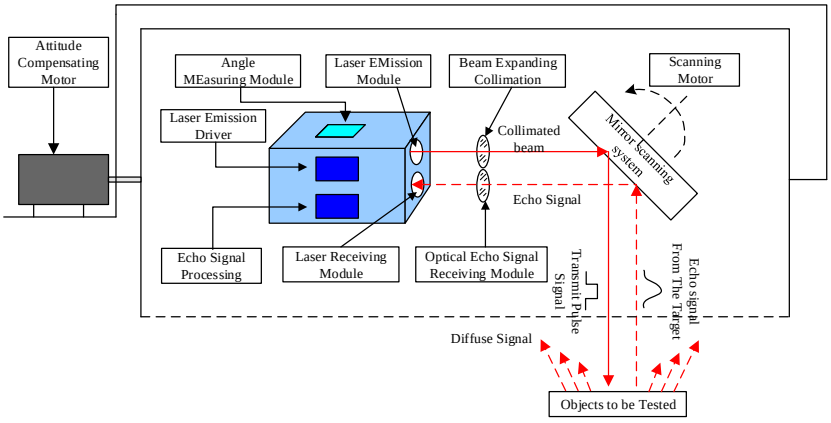

Fig.. 3 Structure and composition of laser 3D scanning elevation measurement system

The laser transmitting unit is composed of trigger signal, semiconductor laser and transmitting optical system; the laser receiving unit is composed of signal amplification circuit composed of transresistance, voltage control and automatic gain, APD detector, receiving optical system and time discrimination module; the laser scanning system is composed of reflector, drive motor and shaft encoder. The data post-processing system consists of data transmission, data processing, AD conversion, microcontroller and FPGA. The integrated system is shown in Fig. 4.

(**a**) Push-brush scanning experimental structure

(**b**) Broom scanning experimental structure

Fig. 4 LiDAR measurement system

Ranging experiments and scanning imaging experiments are carried out through the built experimental platform.

3.2 Processing of geomorphic point cloud data

Data acquisition was carried out on the plane wall, the car fuel tank cap and the complex environment of the campus respectively, to verify the practicability of the algorithm in the actual collection point cloud, and to compare the smoothing effect of the unfiltered surface and the filtering effect of the bilateral filtering algorithm, as shown in Fig. 5. It can be clearly seen from FIG. 6 that in the processing of the planar wall, the model of the bilateral filtered surface has some noise distributed on the surface, but the noise points are processed. The algorithm proposed in this paper has a good processing of these noises, and the model edge is smoother. It can be seen from Fig. 7 that the noise smoothness of the bilateral filter model is coarser than that of the flat wall in the processing of the car fuel tank cap, and there are obvious burrs. From Fig. 9, it can be seen that the bilateral filter model has obvious discrete noise points in both the edge and the center, and the edge lines are not clear because there are burrs on the edge of the object. In contrast, when the geomorphic environment gradually deteriorates and the amplitude gradually increases, the two-sided filtering algorithm gradually loses credibility, and the filtering effect drops precipitously. The algorithm proposed in this paper has a significantly better processing effect on these three models than the bilateral filtering algorithm. The processed point cloud model has no burr points, and the model edge is clearer and smoother, with obvious lines.

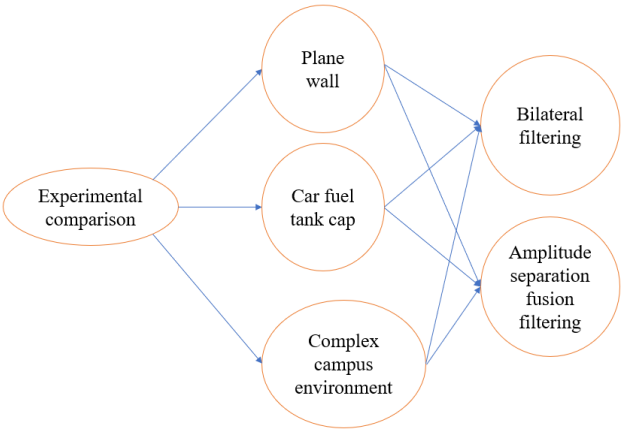

Fig. 5 Comparison of experiments

As shown in Fig. 6, the figure contains the fitting surface of bilateral filtering a, and the fitting surface after amplitude separation and fusion filtering is shown in Fig. b. In terms of smoothing filtering of a planar wall, the filtering effect in this paper is generally consistent with the result obtained by mean filtering, and the result obtained after filtering can be seen from the figure.

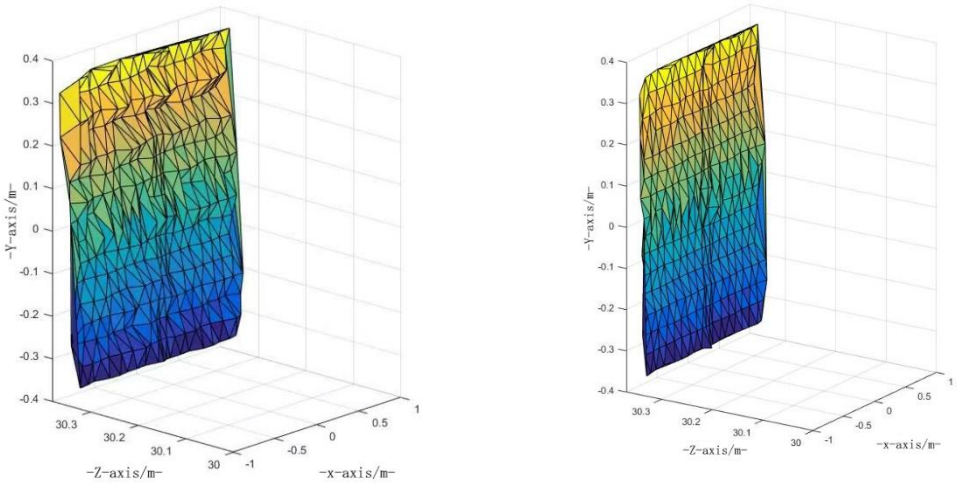

(**a**) Two-sided filter fitted surface

(**b**) The surface is fitted after amplitude separation fusion filtering

Fig. 6 Comparison experiment of planar wall filtering

As shown in Fig. 7, the fairing experiment was conducted on the point cloud model of the base of the car fuel tank cover, and the target was 0.6m away from the liDAR.

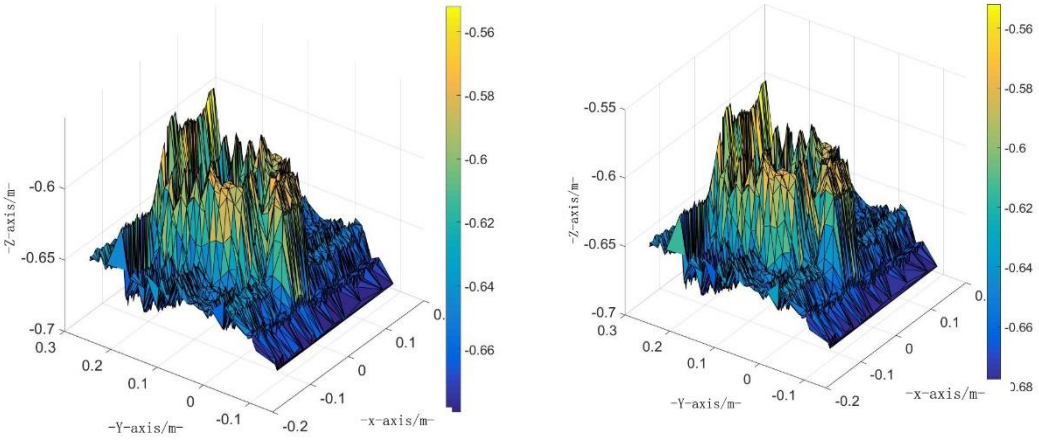

(**a**) The surface of the ground vehicle fuel tank cover base is fitted by double-sided filtering

(**b**) Ground vehicle fuel tank cover base amplitude separation fusion filter fitting surface

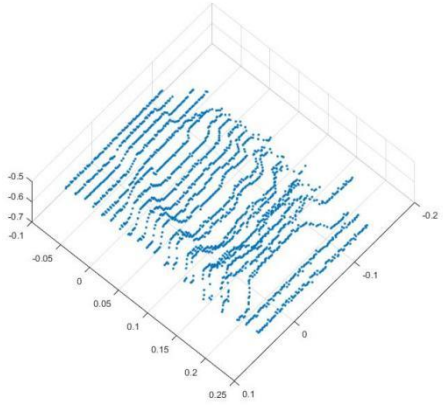

(**c**) Car fuel tank cover base point cloud

(**d**) Car mailbox cover base material

Fig. 7 Smoothing diagram of point cloud model of base of fuel tank cover

The smoothing diagram of the point cloud model of the base of the car fuel tank cover is shown in Fig. 7. The fitting surface of the point cloud by bilateral filtering is shown in Fig. (a); The image with amplitude separation fusion filtering for point cloud is (b); The original point cloud image is Fig. (c). Due to the relatively close distance, the radar acquisition effect is not ideal, and the filtering effect can only be shown from the color intensity. It is not difficult to see that the colors in (b) are more concentrated, which indicates that the filtering is effective.

The environment collected in this paper has the characteristics of geomorphic vibration environment, such as campus water tank, trees, vehicles, uneven terrain environment. The campus geomorphic environment collected by 3D LiDAR is shown in Fig. 8.

Fig. 8 Campus geomorphology collection scene

The point cloud image in Fig. 8 is processed as follows:

(1) The ground target point cloud and the point cloud representing the ground are divided by the point cloud image collected in Fig. 8. See Fig. 9 (a) (b) (c)below.

(2) Through the normal vector estimation of the ground target, the normal vector estimation diagram of the point cloud model is obtained, as shown in Fig. 9(d).

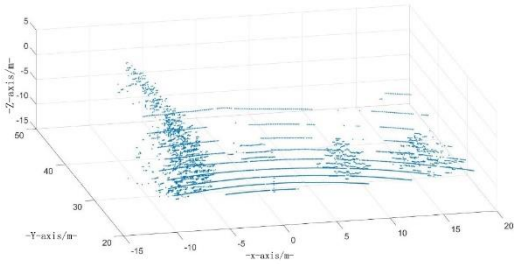

(**a**) Original point cloud image

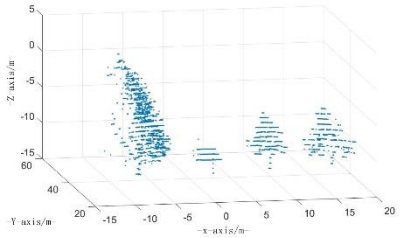

(**b**) Segmented ground target map

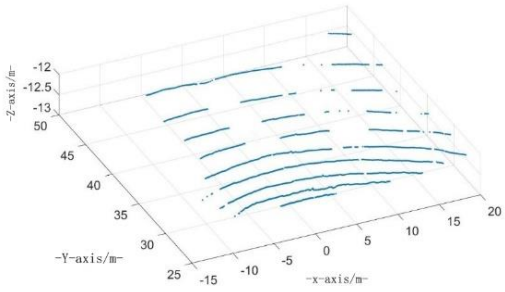

(**c**) The partitioned ground

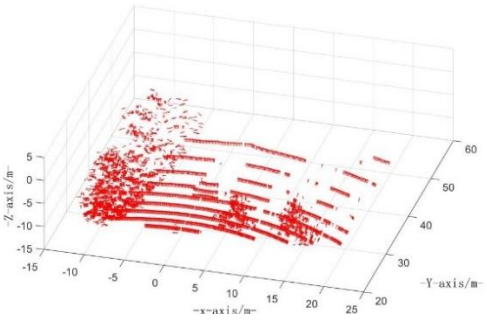

(**d**) Normal vector estimation diagram of point cloud model

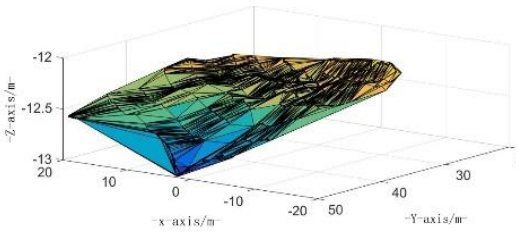

(**e**) Campus landform bilateral filtering effect

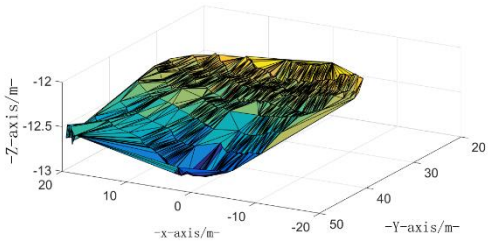

(**f**) Campus landform amplitude separation fusion filter effect

Fig. 9 Fairing map of point cloud processing of campus geomorphology

It can be clearly seen from the effect diagram of Fig.. 9(e)(f) that the effect of the bilateral filtering algorithm is far inferior to that of the amplitude separation fusion algorithm in the case of large values.

It can be clearly seen from Fig.. 6 that in the processing of the planar wall, the model of the bilateral filtered surface has some noise distributed on the surface, but the noise points are processed. The algorithm proposed in this paper has a good processing of these noises, and the model edge is smoother. It can be seen from Fig. 7 that the noise smoothness of the bilateral filter model is coarser than that of the flat wall in the processing of the car fuel tank cap, and there are obvious burrs. From Fig. 9, it can be seen that the bilateral filter model has obvious discrete noise points in both the edge and the center, and the edge lines are not clear because there are burrs on the edge of the object. In contrast, when the geomorphic environment gradually deteriorates and the amplitude gradually increases, the two-sided filtering algorithm gradually loses credibility, and the filtering effect drops precipitously. The composite filtering algorithm proposed in this paper can be seen from FIG. 6, 7, and 9 that the processing of three different models has more uniform noise points, more delicate noise smoothness, clear image edges, and no burrs. Even if the amplitude increases, the uniformity and fineness are still considerable.

3.3 Error calculation of point cloud data

Due to the high measurement accuracy of the LiDAR 3D imaging system, it can be understood that the point cloud data is actually composed of the value of the measured object and the measurement error. In this style, $f\left(x_i,y_i,z_i\right)$ represents the real collected point cloud data, and the point cloud error e is:

$$e\left(x_i,y_i,z_i\right)=f\left(x_i,y_i,z_i\right)-g\left(x_i,y_i,z_i\right) \tag{12}$$

For a more objective verification method, the mean square error MSE is used as a verification reference, which is a measure of the average error:

$$\begin{aligned} MSE_S &= \frac{\sum_q \left|q-q^*\right|^2}{\{q\}} \\ &= \frac{\sum_q ((x_q-x_{q^*})^2+(y_q-y_{q^*})^2+(z_q-z_{q^*})^2}{\left|\{q\}\right|} \end{aligned} \tag{13}$$

Where q is the vertex information that has not been processed by the fairing algorithm, q^* represents the vertex information that has been smoothed and filtered by the filtering algorithm, (x_q,y_q,z_q) is the position of vertex q in the specified coordinate system, $|\{q\}|$ is the total number of point cloud data. The point cloud generated by the unsmoothed data and object simulation method is used as the best collection data of the object object point cloud. After filtering the data and adding the non-optimal collection data in the initial observation point cloud, the resulting errors are shown in Table 1.

Table 1

Error comparison between the two algorithms

Test object	Plane wall			Complex campus			Complex campus environment		
	No composite filtering error	Two-sided filtering algorithm error	Amplitude separation fusion algorithm error	No composite filtering error	Two-sided filtering algorithm error	Amplitude separation fusion algorithm error	No composite filtering error	Two-sided filtering algorithm error	Amplitude separation fusion algorithm error
1	0.3245	0.0235	0.0076	0.5988	0.0867	0.0378	0.7333	0.1555	0.0786
2	0.3556	0.0267	0.0078	0.5123	0.0865	0.0341	0.7578	0.1211	0.0881
3	0.3489	0.0311	0.0069	0.5342	0.0854	0.0400	0.7123	0.1226	0.0723
4	0.3876	0.0288	0.0072	0.5365	0.0941	0.0398	0.7744	0.1567	0.0711
5	0.3179	0.0246	0.0073	0.5428	0.0858	0.0378	0.7788	0.1755	0.7544
6	0.3956	0.0276	0.0076	0.5921	0.0821	0.0411	0.7166	0.1678	0.7433
7	0.3577	0.0265	0.0073	0.5754	0.0787	0.0386	0.7733	0.1744	0.0735
8	0.3911	0.0247	0.0087	0.5214	0.0911	0.0367	0.7113	0.1655	0.0713
9	0.3788	0.0297	0.0081	0.5422	0.0921	0.0391	0.7112	0.1789	0.0812
10	0.3754	0.0211	0.0078	0.5123	0.0858	0.0394	0.7100	0.1756	0.0817

As it can be seen from the above table, the error of the bilateral filtering algorithm is larger when the environment becomes more complex and the large amplitude is more obvious. Especially in the complex campus environment, the error is about 0.15, while the amplitude separation fusion algorithm performs well in the large amplitude with an error of about 0.08. It can be seen that a large number of experiments have proved the reliability and superiority of the amplitude separation fusion algorithm under the condition of large geomorphic amplitude.

3.4 Treatment effect analysis

The number of points and processing time of different models are shown in Table 2. The time complexity of the proposed algorithm is O(K*N), where N is the number of points in the model. The algorithm proposed in this paper performs separation filtering and secondary filtering on the point cloud, so the processing

time is slightly longer than that of the bilateral filtering algorithm. In summary, the algorithm proposed in this paper can effectively deal with the situation of large geomorphic bats, while protecting the sharp features of the model, and restoring the original appearance of the model to the greatest extent.

Table 2

Efficiency processing table

	Bilateral filtering algorithm /s	Amplitude separation fusion algorithm /s
Plane wall	0.567	0.678
Car fuel tank cap	0.778	0.983
Complex campus environment	1.134	1.443

5. Conclusion

In this paper, we apply the mean filter and the two-sided filter and combine the amplitude separation and fusion algorithm to solve the noise problem in the terrain point cloud data. Based on the idea flow of terrain visualization, which first extracts the feature points of the point cloud and then constructs the three-dimensional network structure, the collected data is smootened and smootened by means of combination filter. The average variance MSE of the evaluation index of the synthetic filter is less than 0.09, which can meet the accuracy requirements of point cloud data used for high noise point cloud processing. The idea of separating the large amplitude non-surface and the surface is to separate most of the noise first, and then make the overall two-sided filter, which is very realistic, and successfully overcomes the problem that the two-sided filter is difficult to deal with a lot of noise. Through the analysis of the measured data, compared with the classical bidirectional filter in the three different models, the fusion algorithm based on amplitude separation is smoother and clearer in the processing of large value and large noise, and there are no burrs at the edge and no discrete noise points at the middle edge.

Acknowledgement

This research was funded by Jilin Provincial Science and Technology Development Plan Project (YDZJ202301ZYTS492).

R E F E R E N C E S

[1]. Xing Z.A., Eldon D., Nelson A.O., et al.CAKE: Consistent Automatic Kinetic Equilibrium reconstruction. Fusion Engineering and Design, 2021,163.

[2]. Jianfeng C, Kai Z, Leiyang W, et al. Design of a High Precision Ultrasonic Gas Flowmeter. Sensors, 2020,20(17).

[3]. Zheng L, Yaowu Z, Sijing Z, et al. PCDNF: Revisiting Learning-based Point Cloud Denoising via Joint Normal Filtering. IEEE transactions on visualization and computer graphics, 2023,PP.
[4]. Duan X, Feng L, Zhao X. Point Cloud Denoising Algorithm via Geometric Metrics on the Statistical Manifold. Applied Sciences, 2023,13(14).
[5]. Sun W, Wang J,Jin F, et al. Intelligent Construction Monitoring Method for Large and Complex Steel Structures Based on Laser Point Cloud. Buildings, 2023, 13(7).
[6]. VOLLMERJ, MENCLR, MUELLERH. Improved Laplacian smoothing of noisy surface meshes. Computer Graphics Forum, 2010, 18(3):131-138
[7]. Maletckii B, Yasyukevich Y, Vesnin A. Wave Signatures in Total Electron Content Variations: Filtering Problems. Remote Sensing, 2020,12(8).
[8]. M.G. R,A.S. F,A.J. M, et al. Pulse Transition Time Method for Unobtrusive Blood Pressure Estimation. IFMBE Proceedings, 2020,76.
[9]. Huang Delun, Gao Bo, Bai Hao et al. Application of improved point cloud filtering algorithm in topographic map mapping. Mapping technology and equipment,2022,24(04):65-71.DOI:10.20006/j.cnki.61-1363/P.2022.04.013:2-8.
[10]. Zhou Xuting, Liu Jianqin. Point Cloud Filtering in 3D Point Cloud Measurement. Computer Age, 2022(12):70-72+77.DOI:10.16644/j.cnki.cn33-1094/tp.2022.12.017:8-16.
[11]. Liu Xiangyu, SONG Yu. Multi-scale Point Cloud Filter denoising Method. Beijing Surveying and Mapping, 2022,36(11):1486-1489.DOI:10.19580/j.cnki.1007-3000.2022.11.009:12-16.
[12]. Jiao Yuanbing, Lu Aiping. Improved filtering Algorithm based on airborne LiDAR point Cloud Data. Mapping Standardization, 2022,38(03):42-46.DOI:10.20007/j.cnki.61-1275/P.2022.03.08:3-9.
[13]. Wang C. LiDAR Point Cloud Data Processing and Applications[M].CRC Press:2019-07-15:11-16.
[14]. ZYao Jie, HOU Zhiqun, Zhu Daming et al. Research on an airborne LiDAR point Cloud Combined filtering method. Urban Survey, 2022(04):82-86.
[15]. He Xinxu, Qin Lijuan. Based on voxel filtering algorithm with gaussian filtering algorithm study. Information recording materials, 2022, 23 (7) : 229-231. The DOI: 10.16009 / j.carol carroll nki cn13-1295 / tq. 2022.07.043:4-7.
[16]. Cui Hao, Gao Fei, Yu Min, etc. Airborne LiDAR point cloud filtering algorithm combining CSF and TIN. Journal of Hefei University of Technology (Natural Science Edition),2022,45(05):644-648. (in Chinese).
[17]. Xu Wang, GUAN Yunlan, ZHANG Zhao et al. Airborne LiDAR progressive morphological filtering algorithm combined with thin plate spline interpolation. Advances in Laser and OptoElectronics,202,59(10):412-421. (in Chinese).
[18]. Wang Qiaoli, XU Zengbo, Yang Si. Three-dimensional clothing Modeling based on Scattered Point Cloud. Acta Apparel Sinica, 2019,6(04):366-373. (in Chinese).
[19]. Shan Lijie, Yue Jianping. Automatic extraction algorithm of high voltage tower based on LiDAR point cloud. Advances in Laser and OptoElectronics, 2019,58(24):491-497. (in Chinese).
[20]. Song Wanting, Jiang Wensong, Luo Zai. Rapid batch 3D reconstruction of point clouds based on multi-label classification. Advances in Laser and Optoelectronics, 2019,58(12):75-85. (in Chinese).
[21]. Li Chengkun, Tang Chuyu, Chen Genliang et al. Hull section docking feature recognition based on point cloud matching method. Journal of Marine engineering, lancet, 2021 (6) : 12-17. DOI: 10.13788 / j.carol carroll nki CBGC. 2021.06.03:2-6.